THREE-DIMENSIONAL AND CHAOTIC OSCILLATIONS OF LONG PIPES CONVEYING FLUID IN THE PRESENCE OF AN END-MASS

Yahya Modarres-Sadeghi
Department of Mechanical Engineering, MIT, 77 Massachusetts Ave. Building 5-422 Cambridge MA 02139 USA, modarres@mit.edu

Michael P. Païdoussis
Department of Mechanical Engineering,, McGill University, 817 Sherbrooke W., Montréal, Québec, H3A 2K6, Canada, mary.fiorilli@mcgill.ca

ABSTRACT

Copeland and Moon's experimental results for a long pipe conveying fluid in the presence of a relatively large end-mass have displayed some truly fascinating dynamical behaviour. Theoretical studies, on the other hand, have all dealt with shorter pipes and smaller end-masses, mainly because the convergence of the theoretical results for long pipes with large end-masses is problematic. In this paper, we have been successful to some extent in this regard, and some theoretical results for Copeland and Moon's parameters are presented.

1. INTRODUCTION

The first studies on cantilevered pipes conveying fluid with attached masses were undertaken, using linear models, by Hill and Swanson (1970). This linear work was later continued by Jendrzejczyk and Chen (1985) for a pipe with a mass attached at the free end (here referred to as an "end-mass") and by Sugiyama et al. (1988). These studies showed that the additional mass(es) could either stabilize or destabilize the system *vis-à-vis* the plain pipe, depending on the system parameters and location of the additional mass(es) [see Païdoussis (1998, Section 3.6.3)].

Nonlinear studies of a pipe with an end-mass started mainly after some nonlinear equations for a plain pipe (i.e., without additional masses or springs attached to the pipe) were derived by many researchers (e.g., by Ch'ng and Dowell (1979), Semler et al. (1994) for planar (2-D) motion and by Lundgren et al. (1979), Bajaj et al. (1980), and Rousselet and Herrmann (1981), for three-dimensional (3-D) motion.

The first very interesting nonlinear study on pipes with an end-mass was the experimental work by Copeland and Moon (1992). The experiments were conducted with particularly long, vertically hanging, cantilevered elastomer pipes, fitted at the free end with end-masses of different sizes and showed extremely rich dynamical behaviour, as summarized in Figure 1, where $\Gamma=m_e/[(M+m)L]$, with m_e being the end-mass, M the mass of the fluid per unit length, and m that of the pipe per unit length; $u_g = U/(gL)^{1/2}$ is the dimensionless flow velocity used by Copeland and Moon. In addition to planar and orbital (rotary) motions, an extraordinary array of geometrically more complex motions was discovered. In all cases with an end-mass, for sufficiently high flow velocity the motions became chaotic, often with several intervening periodic oscillatory states. In at least some cases, the quasiperiodic route to chaos was found to be followed. In the analytical part of the study, which was not wholly successful (Copeland, 1992), the long vertical pipes were modelled as hanging strings.

Païdoussis and Semler (1998) studied both theoretically and experimentally the dynamics of more modestly long hanging elastomer cantilevers. In these experiments, the end-mass parameters were considerably smaller than in Copeland and Moon's experiments. Interesting observations were made in this case also. Planar flutter was followed by a secondary bifurcation as the flow velocity was increased, which could be identified with a sudden and substantial increase in the frequency, accompanied by a peculiar mode of oscillation with a seemingly stationary node around the mid-length. For higher flow velocities, the motion eventually became chaotic and three-dimensional.

Païdoussis and Semler's (1998) experimental results were compared to the theoretical ones, obtained with their 2-D model. The Hopf and secondary bifurcations were reasonably well predicted, as was the transition to chaos. See Païdoussis (1998, Section 5.8.3) for an extensive review on nonlinear work on pipes with an end-mass.

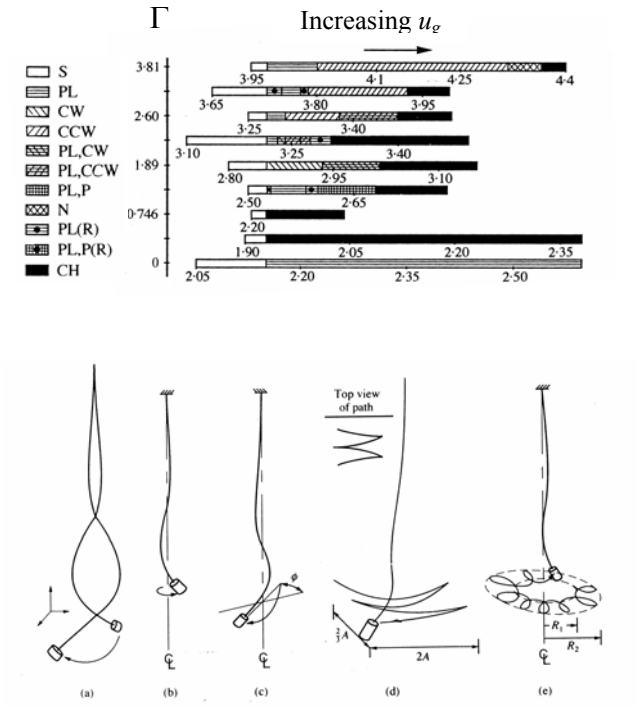

Figure 1. Transition from equilibrium to chaos for 3-D motions of the system for various end-masses. Top: the ranges of various oscillatory states in terms of increasing u_g *for different end-masses,* Γ*. S: stationary tube; PL: planar oscillation; CW: clockwise rotating motion; CCW: counter-clockwise rotating motion; PL, CW: clockwise rotating planar oscillation; PL, CCW: counter-clockwise rotating planar oscillation; PL(R): planar oscillation rotating through a finite angle; PL, P: coupled planar and pendular oscillation; PL, P(R): coupled oscillation and pendular oscillation rotating through a finite angle; N: nutation; CH: chaos. Bottom: sketches of various periodic motions. (a) PL; (b) CCW; (c) PL(R); (d) PL, P; (e) N [Copeland and Moon (1992)].*

A 3-D version of the nonlinear equations of motion of Semler et al. (1994) is derived by Wadham-Gagnon et al. (2007). These equations have been used successfully (Modarres-Sadeghi et al., 2007) to study the three-dimensional behaviour of a pipe with an end-mass and with physical properties of the pipe as in Païdoussis and Semler's (1998) experiments. In the same paper, it was shown that the convergence of the 3-D theoretical results for cases with large gravitational parameter (γ; proportional to the length cubed) and end-mass parameter (Γ) is not easily obtainable. In the present paper, the 3-D study of pipes with end-masses is extended to the range of the pipes used in Copeland and Moon's experiments (1992).

2. THEORETICAL MODEL

The equations of motion have been derived by Wadham-Gagnon et al. (2007) for a general case where there are some intermediate springs as well as an end-mass attached to the pipe. For the present study, all terms related to the intermediate springs have been deleted. The resulting dimensionless form of these equations is

$$\begin{aligned}
&\eta^{(4)}+\left[1+\Gamma\delta(\xi-1)\right]\ddot{\eta}+2u\sqrt{\beta}\,\dot{\eta}'+u^2\eta''+\gamma\left[1+\Gamma\delta(\xi-1)\right]\eta'\\
&+\gamma\eta''\int_\xi^1\left[1+\Gamma\delta(\xi-1)\right]\mathrm{d}\xi\\
&+\gamma\left[1+\Gamma\delta(\xi-1)\right]\left(\tfrac{1}{2}\eta'^3+\tfrac{1}{2}\eta'\zeta'^2\right)\\
&-\gamma\left(\tfrac{3}{2}\eta'^2\eta''+\tfrac{1}{2}\eta'\zeta'^2+\eta'\zeta'\zeta''\right)\int_\xi^1\left[1+\Gamma\delta(\xi-1)\right]\mathrm{d}\xi\\
&+2u\sqrt{\beta}\left[\eta'^2\dot{\eta}'+\eta'\zeta'\dot{\zeta}'-\eta''\int_\xi^1\left(\eta'\dot{\eta}'+\zeta'\dot{\zeta}'\right)\mathrm{d}\xi\right]\\
&+u^2\left[\eta'^2\eta''+\eta'\zeta'\zeta''-\eta''\int_\xi^1\left(\eta'\dot{\eta}'+\zeta'\dot{\zeta}'\right)\mathrm{d}\xi\right]\\
&+\left(\eta'^2\eta^{(4)}+4\eta'\eta''\eta'''+\eta''^3+\eta'^2\zeta'\zeta^{(4)}+3\eta'\zeta''\zeta'''+\eta''\zeta'\zeta'''+\eta''\zeta''^2\right)\\
&+\eta'\left[1+\Gamma\delta(\xi-1)\right]\int_0^\xi\left(\dot{\eta}'^2+\eta'\ddot{\eta}'+\dot{\zeta}'^2+\zeta'\ddot{\zeta}'\right)\mathrm{d}\xi\\
&-\eta''\int_\xi^1\left[1+\Gamma\delta(\xi-1)\right]\int_0^\xi\left(\dot{\eta}'^2+\eta'\ddot{\eta}'+\dot{\zeta}'^2+\zeta'\ddot{\zeta}'\right)\mathrm{d}\xi\mathrm{d}\xi+O\left(\varepsilon^4\right)=0,
\end{aligned}\tag{1}$$

$$\begin{aligned}
&\zeta^{(4)}+\left[1+\Gamma\delta(\xi-1)\right]\ddot{\zeta}+2u\sqrt{\beta}\,\dot{\zeta}'+u^2\zeta''+\gamma\left[1+\Gamma\delta(\xi-1)\right]\zeta'\\
&+\gamma\zeta''\int_\xi^1\left[1+\Gamma\delta(\xi-1)\right]\mathrm{d}\xi\\
&+\gamma\left[1+\Gamma\delta(\xi-1)\right]\left(\tfrac{1}{2}\zeta'^3+\tfrac{1}{2}\zeta'\eta'^2\right)\\
&-\gamma\left(\tfrac{3}{2}\zeta'^2\zeta''+\tfrac{1}{2}\zeta'\eta'^2+\zeta'\eta'\eta''\right)\int_\xi^1\left[1+\Gamma\delta(\xi-1)\right]\mathrm{d}\xi\\
&+2u\sqrt{\beta}\left[\zeta'^2\dot{\zeta}'+\zeta'\eta'\dot{\eta}'-\zeta''\int_\xi^1\left(\zeta'\dot{\zeta}'+\eta'\dot{\eta}'\right)\mathrm{d}\xi\right]\\
&+u^2\left[\zeta'^2\zeta''+\zeta'\eta'\eta''-\zeta''\int_\xi^1\left(\zeta'\dot{\zeta}'+\eta'\dot{\eta}'\right)\mathrm{d}\xi\right]\\
&+\left(\zeta'^2\zeta^{(4)}+4\zeta'\zeta''\zeta'''+\zeta''^3+\zeta'^2\eta'\eta^{(4)}+3\zeta'\eta''\eta'''+\zeta''\eta'\eta'''+\zeta''\eta''^2\right)\\
&+\zeta'\left[1+\Gamma\delta(\xi-1)\right]\int_0^\xi\left(\dot{\zeta}'^2+\zeta'\ddot{\zeta}'+\dot{\eta}'^2+\eta'\ddot{\eta}'\right)\mathrm{d}\xi\\
&-\zeta''\int_\xi^1\left[1+\Gamma\delta(\xi-1)\right]\int_0^\xi\left(\dot{\zeta}'^2+\zeta'\ddot{\zeta}'+\dot{\eta}'^2+\eta'\ddot{\eta}'\right)\mathrm{d}\xi\mathrm{d}\xi+O\left(\varepsilon^4\right)=0,
\end{aligned}\tag{2}$$

where the dimensionless parameters are

$$\xi=\frac{s}{L},\quad \eta=\frac{v}{L},\quad \zeta=\frac{w}{L},\quad \tau=\left(\frac{EI}{m+M}\right)^{1/2}\frac{t}{L^2},$$
$$u=\left(\frac{\rho A}{EI}\right)^{1/2}UL,\quad \beta=\frac{\rho A}{m+\rho A},\quad \gamma=\frac{(m-\rho A)gL^3}{EI},$$
$$\Gamma=\frac{m_e}{(m+M)L},\qquad (3)$$

in which η and ζ are mutually orthogonal dimensionless transverse displacements, u is the dimensionless flow velocity, γ the dimensionless gravity parameter, β a mass parameter, Γ the dimensionless end-mass parameter, and τ the dimensionless time. In Eqs. (3), s is the distance along the pipe, measured from the clamped end, L is the length of the pipe, D its diameter and EI its flexural rigidity; ρ is the density of the fluid, m the mass per unit length of the pipe, M the mass per unit length of the fluid, U the dimensional flow velocity, and m_e the end-mass. The transverse displacements are of order ε.

This dimensionless set of nonlinear partial differential equations is discretized to a series of ODEs via Galerkin's technique with the eigenfunctions of a plain cantilevered beam as the basis functions. The resulting set of ordinary differential equations is then solved by Houbolt's finite difference method (Semler et al., 1996) and AUTO (Doedel and Kernéves, 1986), utilizing appropriate initial conditions and fine enough time steps. For a detailed discussion on the methods of solution see Modarres-Sadeghi (2006). The results shown in this paper are obtained by using 8 modes each in η and ζ directions (16 modes in total).

3. RESULTS

Physical properties of the pipe used in Copeland and Moon's experiments are given in Tables 1 and 2. They conducted the experiments for the pipe with no end-mass (plain pipe) as well as the pipe with eight different end-masses. For every case, the pipe lost its initial static stability by a Hopf bifurcation leading to flutter at some critical flow velocity, u_{HB}. The ensuing dynamics depends on the value of the end-mass as can be observed in Figure 1. We have conducted the theoretical analysis for all these 9 cases and we discuss the results in what follows.

For the case with no end-mass, our theoretical results, in agreement with Copeland and Moon's observations, show planar oscillation after the loss of stability. This has been studied in detail in Modarres-Sadeghi et al. (2008), where it is shown that, if one does not take into account the influence of gravity, a three-dimensional oscillation is predicted, which is not what occurs physically. With a non-zero gravity parameter, however, we have observed a planar periodic motion, which remains periodic with no secondary bifurcation point, the same as in Copeland and Moon's observations.

Length, L	0.989 m
Inner/outer diameter, D_i/D_o	7.94 / 15.85 mm
Flexural rigidity, EI	7.28×10^{-3} N·m^2
Density of the pipe, ρ_p	1167 kg/m^3
Density of the fluid, ρ_f	999 kg/m^3
Mass per unit length of pipe, m	0.177 kg/m
Mass per unit length of fluid, M	0.04951 kg/m

Table 1. Pipe parameters used in the calculation

Dimensionless mass parameter, β	0.2186
Dimensionless gravity parameter, γ	295.27
Dimensionless end-mass parameter, Γ	0.367 … 3.81

Table 2. Dimensionless parameters used in the calculation

The interesting dynamics is observed in the presence of an end-mass. Overall, similarly to what Copeland and Moon observed in their experiments, the pipe loses stability by a Hopf bifurcation at some critical flow velocity. This critical flow velocity increases as larger end-masses are used. In all cases, the Hopf bifurcation is found to be *subcritical*, in agreement with Copeland and Moon experimental observations. Depending on the initial conditions used in FDM, one can find zero or nonzero solutions for flows lower than the critical. The periodic oscillations are then followed by period-2, -4, -n oscillations in some cases and quasiperiodic oscillations in some other cases; both are routes leading to chaos at higher flow velocities. Figure 2 shows the critical flow velocities for the Hopf bifurcation (onset of periodic oscillations according to a linear prediction), limit point (threshold of periodic motions according to nonlinear theory) and the onset of chaotic oscillations. It is observed that for large end-mass parameters, chaotic oscillations start even before the Hopf bifurcation point. The Hopf bifurcation is subcritical and therefore periodic motions start at flow velocities lower than the critical flow for the Hopf bifurcation. Then, the transition from periodic

to chaotic oscillations occurs so quickly that it is possible to observe chaotic oscillations even before the critical flow velocity for the Hopf bifurcation. This means that for a range of flow velocities, depending on the initial conditions, the pipe will either go to its static equilibrium position or display chaotic oscillations. It should be mentioned here that the first point of instability, a double Hopf bifurcation point, is found by AUTO very accurately. However, AUTO cannot follow the stable solutions following a double Hopf bifurcation; therefore all the nonzero stable results are obtained by FDM.

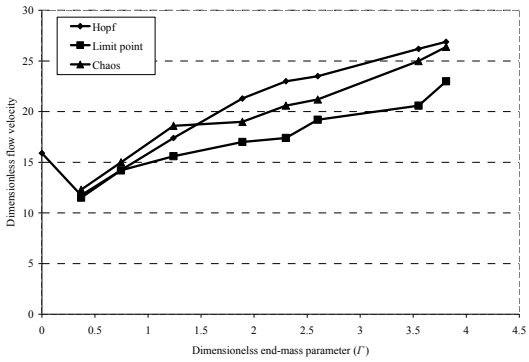

Figure 2. Critical flow velocities of Hopf bifurcation, limit point and the onset of chaos for various end-mass parameters.

For the two smallest end-mass parameters in Copeland and Moon's experiments, Γ= 0.37 and Γ = 0.746, we find a quasiperiodic route to chaos. The succession from periodic to chaotic motion is so quick (see Figure 2) that Copeland and Moon reported the onset of chaos immediately following the static equilibrium solution. Figure 3 shows a periodic solution for Γ =0.367 and u=11.6, where the pipe oscillates on a curved path. The first two rows of this figure show time histories and phase-plane plot of the pipe oscillations in two perpendicular directions. The solo plot in the last row shows the top view of the tip motion. At higher flow velocities, quasiperiodic oscillations are obtained which are followed by chaotic oscillations at even higher flows.

The difference between the critical points for the limit point and the onset of chaos in Figure 2 gives the range for which the periodic or quasiperiodic oscillations could have been observed in the experimental case. This range widens as the end-mass increases and this can be thought of as the reason that Copeland and Moon were able to observe some periodic or quasiperiodic oscillations in the cases with larger end-mass parameter.

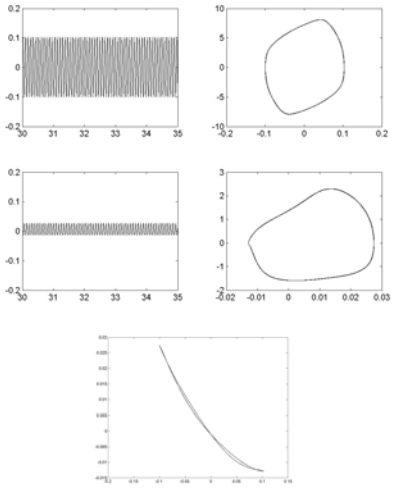

Figure 3. Periodic solution for Γ *= 0.367 and u=11.6. Fist row from left:* η *versus* τ *;* $\dot{\eta}$ *versus* η*. Second row same as first, but for* ζ*. Third row:* ζ *versus* η*.*

For large end-mass parameters, where Copeland and Moon have reported various kinds of planar and three-dimensional oscillations (some quite intricate), our theoretical results have shown similar behaviour. As an example, for Γ = 1.24, oscillations are initially planar in both experiment and in theory. The planar oscillation is then followed by what Copeland and Moon call "coupled planar and pendular oscillations" and this is what we have obtained theoretically, as shown in

Figure 4 for u = 16.2, where a period-4 oscillation is observed. This case shows a period-doubling route to chaos.

In some cases and for some flow velocities, the pipe undergoes a planar motion which rotates within a limited angle. Figure 5 shows this motion for Γ=2.3 and u=18.8. Copeland and Moon observed this kind of motion for their experimental run with Γ=2.3. We have also been able to observe planar motions, which rotate in clockwise or counter-clockwise directions in cases with larger end-masses. Figure 6 shows an example of counter-clockwise planar oscillations for the case with Γ = 3.55 at u = 24.6.

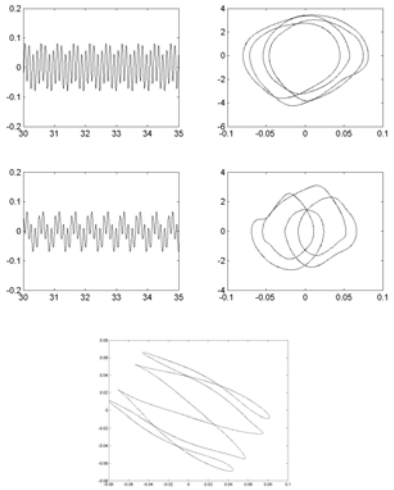

Figure 4. Period-4 solution for Γ *=1.24 and u=16.2.*

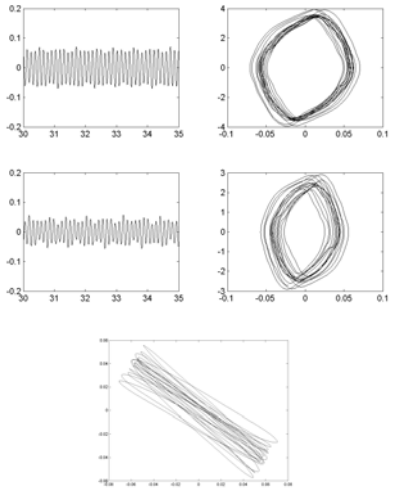

Figure 5. Planar motion within a limited angle for Γ *=2.3 and u=18.8.*

Chaotic oscillations are obtained at high flows for all mass parameters, as Copeland and Moon have observed. Again, similarly to their experimental observations, the critical point for the onset of chaos increases with the end-mass parameter.

Table 3 gives a summary of types of oscillations observed theoretically for various end-mass parameters at various flow velocities. Numerical values for the theoretical critical points are smaller than those observed experimentally. This may be attributed to the existence of imperfections in the pipe used in the experiments, as well as to the fact that the end-mass is considered as a point-mass and also to the assumptions made in the theoretical model (for example, that the equations are correct to $O(\varepsilon^3)$, while with large amplitude motions, we might need higher-order models).

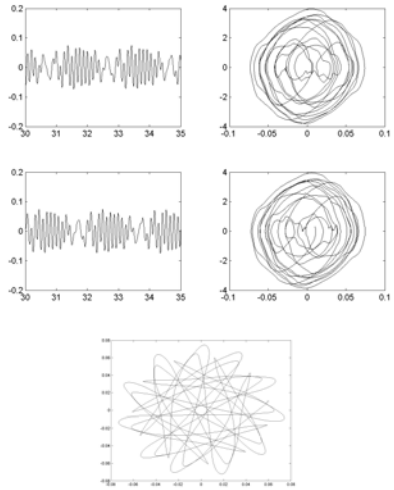

Figure 6. Oscillations for Γ *=3.55 and u=24.6.*

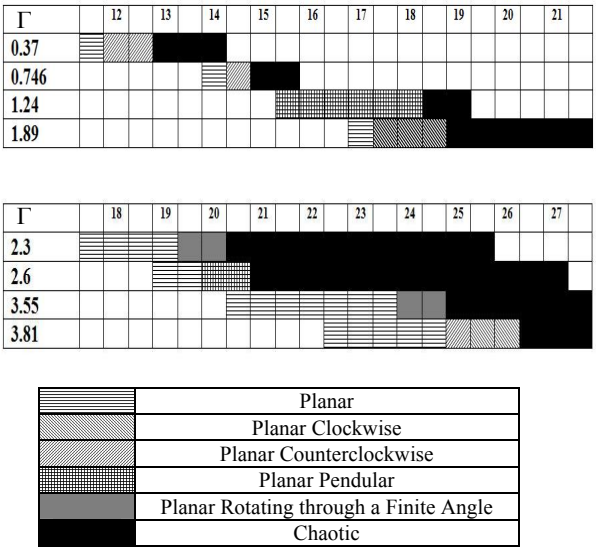

Table 3. Types of oscillations observed at various flow velocities and with various end-mass parameters, found theoretically.

4. CONCLUSION

Some theoretical results are presented for a long pipe with an end-mass used by Copeland and Moon in their experimental study. It was shown previously that achieving convergence of theoretical results for the dimensionless parameters corresponding to Copeland and Moon's experiment is not a trivial task. A newly developed three-dimensional model is used, a relatively large number of modes has been used in Galerkin discretization of the partial difference equation, and extra care has been taken in choosing the initial conditions and time steps in the finite difference method used in the numerical calculations.

It is shown that the pipe loses initial stability by a double Hopf bifurcation, similarly to Copeland and Moon's observation. The resulting periodic motions are followed by period-doubling or quasiperiodic routes to chaos depending on the end-mass parameter. The critical values for the Hopf bifurcation and that for the onset of chaos increase with the end-mass parameter. The theoretical results reproduce some of the rich dynamics observed by Copeland and Moon in their experiments, including coupled planar and pendular oscillations, planar oscillations rotating through a finite angle, and planar motions rotating clockwise or counter-clockwise.

5. REFERENCES

Bajaj, A.K., Sethna, P.R., Lundrgren, T.S., 1980. Hopf bifurcation phenomena in tubes carrying fluid. SIAM Journal of Applied Mathematics 39, 213-230.

Copeland, G.S., 1992. Flow-induced vibration and chaotic motion of a slender tube conveying fluid. Ph.D. dissertation, Cornell University, Ithaca, NY, U.S.A.

Copeland, G.S. & Moon, F.C., 1992. Chaotic flow-induced vibration of a flexible tube with end mass, Journal of Fluids and Structures 6, 705-718; also in American Society of Mechanical Engineers AMD-152 8, 63-77.

Ch'ng E., Dowell, E.H., 1979. A theoretical analysis of nonlinear effects on the flutter and divergence of a tube conveying fluid. Flow-Induced Vibrations, Eds. S.S. Chen & M.D. Bernstein, 65-81. ASME, New York.

Doedel, E.J., Kernéves, J.P. 1986. AUTO: software for continuation and bifurcation problems in ordinary differential equations. Applied Mathematics Report, California Institute of Technology, Pasadena, California, U.S.A. (procurable from doedel@cs.concordia.ca)

Hill J. L., Swanson, C. P., 1970. Effects of lumped masses on the stability of fluid conveying tubes. Journal of Applied Mechanics 37, 494-497.

Jendrzejczyk, J.A., Chen, S.S., 1985. Experiments on tubes conveying fluid. Thin Walled Structures 3, 109-134

Lundgren, T.S., Sethna, P.R.,. Bajaj, A.K., 1979. Stability boundaries for flow induced motions of tubes with an inclined terminal nozzle. Journal of Sound and Vibration 64, 553-571.

Modarres-Sadeghi, Y. 2006. Nonlinear dynamics of a slender flexible cylinder subjected to axial flow. PhD Thesis, McGill University.

Moddares-Sadeghi, Y., Semler, C., Wadham-Gagnon, M., Païdoussis, M.P., 2007. Dynamics of cantilevered pipes conveying fluid, Part 3: three-dimensional dynamics in the presence of an end-mass. Journal of Fluids and Structures, 23, 589-603.

Modarres-Sadeghi, Y., Païdoussis, M.P., Semler, C., 2008. Three-dimensional oscillations of a cantilever pipe conveying fluid. International Journal of Non-Linear Mechanics, 43, 18-25.

Païdoussis, M.P., 1998. Fluid-Structure Interactions: Slender Structures and Axial Flow, Volume 1. Academic Press, London.

Païdoussis, M. P., Semler, C., 1998. Non-linear dynamics of a fluid-conveying cantilevered pipe with a small mass attached at the free end. Journal of Non-Linear Mechanics 33, 15-32.

Rousselet, J., Hermann, G., 1981. Dynamic behaviour of continuous cantilevered pipes conveying fluid near critical velocities. Journal of Applied Mechanics 48, 943-947.

Semler, C., Li G. X., Païdoussis, M. P., 1994. The non-linear equations of motion of pipes conveying fluid. Journal of Sound and Vibration 169, 577-599.

Semler, C., Gentleman, W. C., Païdoussis, M. P., 1996. Numerical solutions of second-order implicit ordinary differential equations. Journal of Sound and Vibration 195, 553-574

Wadham-Gagnon, M., Païdoussis, M. P., Semler, C., 2007. Dynamics of cantilevered pipes conveying fluid, part 1: nonlinear equations of three-dimensional motion. Journal of Fluids and Structures, 545-567.

Sugiyama, Y., Kawagoe, H., Kishi, T., Nishiyama, S., 1988. Studies on the stability of pipes conveying fluid (the combined effect of a spring support and a lumped mass). JSME International Journal, Series 1, 31, 20-26.